ORNL-4908
(ENDF-204)

cy 1

^{63}Cu AND ^{65}Cu NEUTRON ELASTIC AND INELASTIC SCATTERING CROSS SECTIONS FROM 5.50 TO 8.50 MeV

W. E. Kinney
F. G. Perey

OAK RIDGE NATIONAL LABORATORY
OPERATED BY UNION CARBIDE CORPORATION • FOR THE U.S. ATOMIC ENERGY COMMISSION

Printed in the United States of America. Available from
National Technical Information Service
U.S. Department of Commerce
5285 Port Royal Road, Springfield, Virginia 22151
Price: Printed Copy $4.00; Microfiche $0.95

ORNL-4908
UC-79d
(ENDF-204)

Contract No. W-7405-eng-26

Neutron Physics Division

^{63}Cu AND ^{65}Cu NEUTRON ELASTIC AND INELASTIC SCATTERING CROSS SECTIONS FROM 5.50 TO 8.50 MeV

W. E. Kinney and F. G. Perey

FEBRUARY 1974

OAK RIDGE NATIONAL LABORATORY
Oak Ridge, Tennessee 37830
operated by
UNION CARBIDE CORPORATION
for the
U.S. ATOMIC ENERGY COMMISSION

CONTENTS

^{63}Cu AND ^{65}Cu NEUTRON ELASTIC AND INELASTIC SCATTERING CROSS SECTIONS FROM 4.07 TO 8.50 MeV

W. E. Kinney and F. G. Perey

ABSTRACT

Measured neutron elastic and inelastic scattering cross sections for ^{63}Cu and ^{65}Cu between 5.50 and 8.50 MeV are presented and compared with elastic data of Holmqvist and Wiedling[2] and with ENDF/B III MAT 1085 and 1086. Our elastic differential cross sections are in fair agreement with those of Holmqvist and Wiedling in shape. Our angle-integrated differential elastic cross sections are systematically higher by as much as 28% than those of Holmqvist and Wiedling above 5 MeV, a situation similar to that found in comparing the two sets of data for other elements. ENDF/B III MAT 1085 and 1086 angular distributions underestimate the elastic forward peak below 20 deg. when compared with experimental results and display unphysical fluctuations due to the use of a Legendre series of order 20 where order 9 is the highest required by the data. An evaporation model with temperature ranging from 0.8 to 1.05 MeV reasonably describes inelastic scattering to levels in the residual copper nuclei of excitation energy above 3.2 MeV.

INTRODUCTION

The data reported here are the results of one of a series of experiments to measure neutron elastic and inelastic scattering cross sections at the ORNL Van de Graaffs. Reports in the series are listed in Reference 1. This report presents measured neutron elastic and inelastic scattering cross sections for ^{63}Cu and ^{65}Cu from 5.50 to 8.50 MeV. To assist in the evaluation of the data, the data acquisition and reduction techniques are first briefly discussed. For the purposes of discussion the data are presented in graphical form and are compared with the results of Holmqvist and Wiedling[2] and with ENDF/B III (Evaluated Neutron Data File B, Version III) MAT 1085 and 1086. Tables of numerical values of the elastic scattering cross sections and cross sections for inelastic scattering to discrete levels in the residual nucleus are given in an appendix.

DATA ACQUISITION

The data were obtained with conventional time-of-flight techniques. Pulsed (2 MHz), bunched (approximately 1.5 nsec full width at half maximum, FWHM) deuterons accelerated by the ORNL Van de Graaffs interacted with deuterium in a gas cell to produce neutrons by the D(d,n)^{3}He reaction. The gas cells, of length 1 and 2 cm, were operated at pressures of approximately 1.5 atm and gave neutron energy resolutions of the order of $\pm$60 keV.

The neutrons were scattered from solid right circular cylindrical samples of ^{63}Cu and ^{65}Cu placed approximately 10 cm from the gas cells when the detector angles were greater than 25 degrees. For smaller detector angles the cell-to-sample distance had to be increased to 33 cm in order to shield the detectors from neutrons coming directly from the gas cells. the ^{63}Cu sample was 2.00 cm in diameter, 2.20 cm in height, with a mass of 52.43 gm. The ^{65}Cu sample was also 2.00 cm in diameter, and 2.20 cm in height, but had a mass of 50.14 gm.

The scattered neutrons were detected by 12.5 cm diameter NE-213 liquid scintillators optically coupled to XP-1040 photomultipliers. The scintillators were 2.5 cm thick. Data were taken with three detectors simultaneously. Flight paths were approximately 4 m with the detector angles ranging from 15 to 140 degrees. The gas cell neutron production was monitored by a time-of-flight system which used a 5 cm diameter by 2.5 cm thick NE-213 scintillator viewed by a 56-AVP photomultiplier placed about 4 m from the cell at an angle of 55 degrees with the incident deuteron beam.

For each event a PDP-7 computer was given the flight time of a detected recoil proton event with reference to a beam pulse signal, the pulse height of the recoil proton event, and identification of the detector. The electronic equipment for supplying this information to the computer consisted, for the most part, of standard commercial components. The electronic bias was set at approximately 700 keV neutron energy to ensure good pulse shape discrimination against gamma-rays at all energies.

The detector efficiencies were measured by (n,p) scattering from a 6 mm diameter polyethylene sample and by detecting source $D(d,n)^3He$ neutrons at 0 degrees[3]. Both interactions gave results which agreed with each other and which yielded efficiency versus energy curves that compared well with calculations[4].

DATA REDUCTION

Central to the data reduction process was the use of a light pen with the PDP-7 computer oscilloscope display programs to extract peak areas from spectra. The light pen made a comparatively easy job of estimating errors in the cross section caused by extreme but possible peak shapes.

The reduction process started by normalizing a sample-out to a sample-in time-of-flight spectrum by the ratio of their monitor neutron peak areas, subtracting the sample-out spectrum, and transforming the difference spectrum into a spectrum of center-of-mass cross section versus excitation energy. This transformation allowed ready comparison of spectra taken at different angles and incident neutron energies by removing kinematic effects. It also made all single peaks have approximately the same shape and width regardless of excitation energy (in a time-of-flight spectrum, single peaks broaden with increasing flight time). A spectrum of the variance based on the counting statistics of the initial data was also computed. Figure 1 shows a typical time-of-flight spectrum and its transformed energy spectrum.

The transformed spectra were read into the PDP-7 computer and the peak stripping was done with the aid of the light pen. A peak was stripped by drawing a background beneath it, subtracting the background, and calculating the area, centroid, and FWHM of

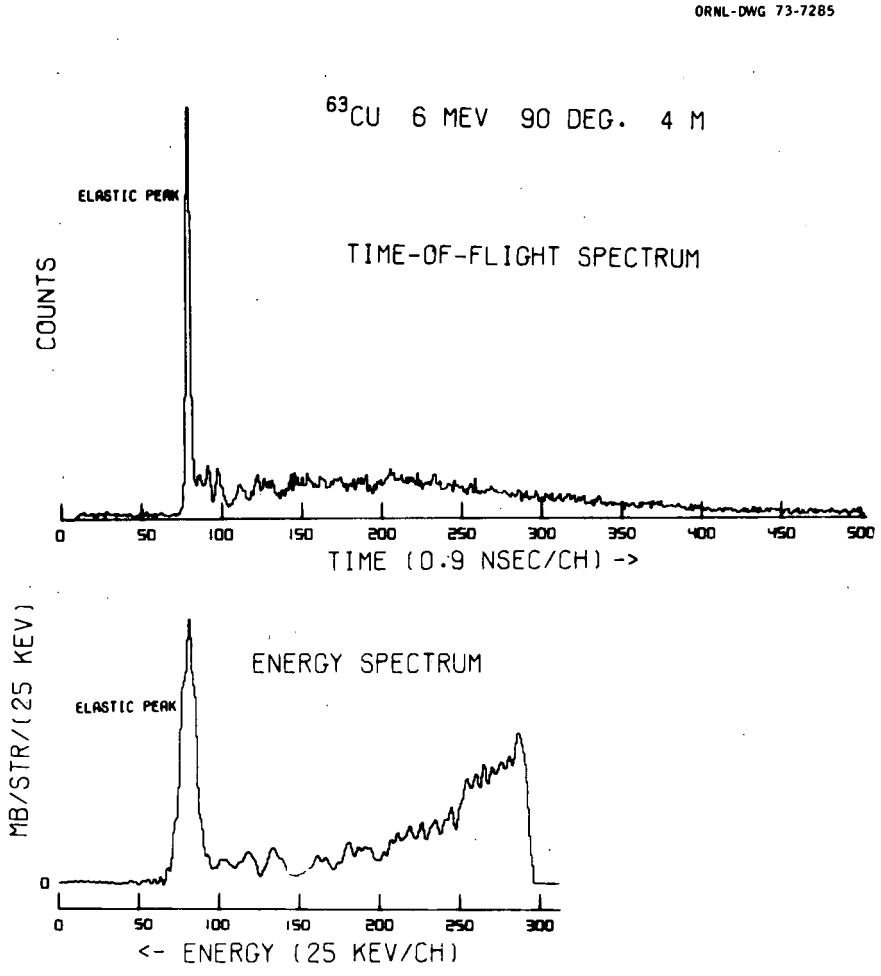

Fig. 1. A typical ^{63}Cu time-of-flight spectrum with its transformed energy spectrum. The data were taken at an incident neutron energy of 6.00 MeV and at an angle of 90 deg. with a flight path of 4 m. Note that the energy spectrum has been offset to allow negative excursions due to statistics in the subtraction of the sample-out background.

the difference. The variance spectrum was used to compute a counting statistics variance corresponding to the stripped peak. Peak stripping errors due to uncertainties in the residual background under the peaks or to the tails of imperfectly resolved nearby peaks could be included with the other errors by stripping the peaks several times corresponding to high, low, and best estimates of this background. Although somewhat subjective, the low and high estimates of the cross sections were identified with 95% confidence limits; these, together with the best estimate, defined upper and lower errors due to stripping. When a spectrum was completely stripped, the output information was written on magnetic tape for additional processing by a large computer.

Finite sample corrections were performed according to semianalytic recipes whose constants were obtained from fits to Monte Carlo results[5]. The corrections were 7 - 8% in the forward peak, 40 - 60% in the first minimum, and 13 - 15% on the second maximum.

The final error analysis included uncertainties in the geometrical parameters (scatterer size, gas cell-to-scatterer distance, flight paths, etc.) and uncertainties in the finite sample corrections.

The measured differential elastic scattering cross sections were fitted by least squares to a Legendre series:

$$\sigma(\mu = \cos\theta) = \Sigma[(2k+1)/2]a_k P_k(\mu)$$

the points being weighted by the inverse of their variances which were computed by squaring the average of the upper and lower uncertainties. The common 7% uncertainty in absolute normalization was not included in the variances for the fitting. In order to prevent the fit from giving totally unrealistic values outside the angular range of our measurements, we resorted to the inelegant but workable process of adding three points equally spaced in angle between the largest angle of measurement and 175 degrees. The differential cross sections at the added points were chosen to approximate the diffraction pattern at large angles, but were assigned 50% errors.

RESULTS

Elastic Scattering Differential Cross Sections

Our differential elastic scattering cross sections for ^{63}Cu and ^{65}Cu are shown in Figures 2 and 3, respectively, along with Legendre least squares fits to the data. Wick's Limit is shown and was used in the fitting.

Both our ^{63}Cu and ^{65}Cu differential elastic scattering cross sections are compared with the natural copper results of Holmqviist and Wiedling[2] in Figures 4 and 5.The ENDF/B III MAT 1086 angular distributions normalized to integrals of the experimental data are also shown.

The ENDF/B III MAT 1086 is the ^{65}Cu evaluation but ENDF/B III MAT 1085, which is the ^{63}Cu evaluation, has the same angular distributions as ENDF/B III MAT 1086. The ENDF/B III MAT 1086 angular distributions are described by a Legendre series of order 20.

It might first be noted that our ^{63}Cu and ^{65}Cu data generally agree within experimental uncertainties. Our results at 7.00 $\pm$ 0.06 MeV appear to agree with the measurements of

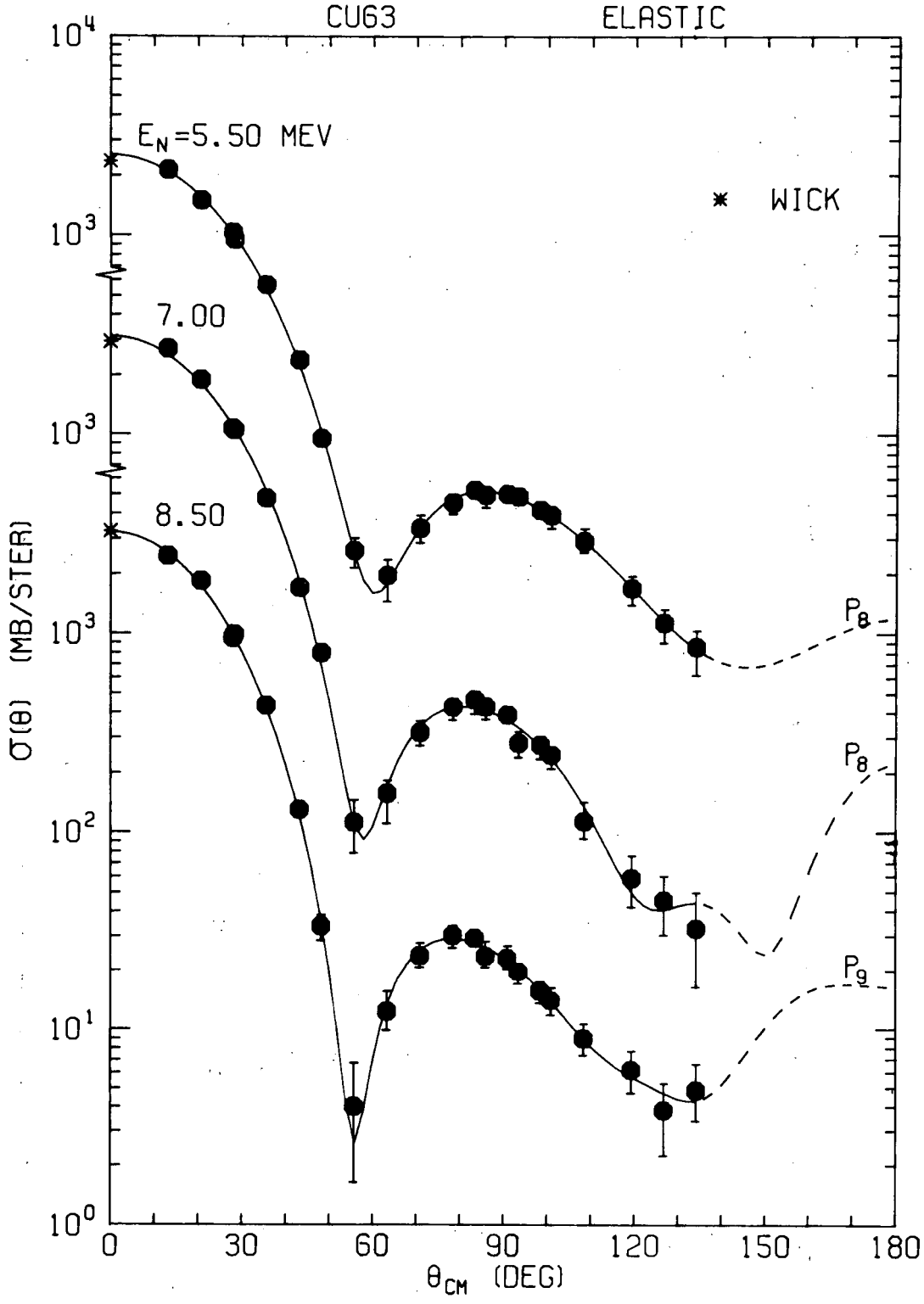

Fig. 2. Our ^{63}Cu neutron differential elastic center-of-mass scattering cross sections with Legendre fits to the data. WICK indicates Wick's Limit which was used in the fitting. The 7% uncertainty in absolute normalization common to all points is not included in the error bars.

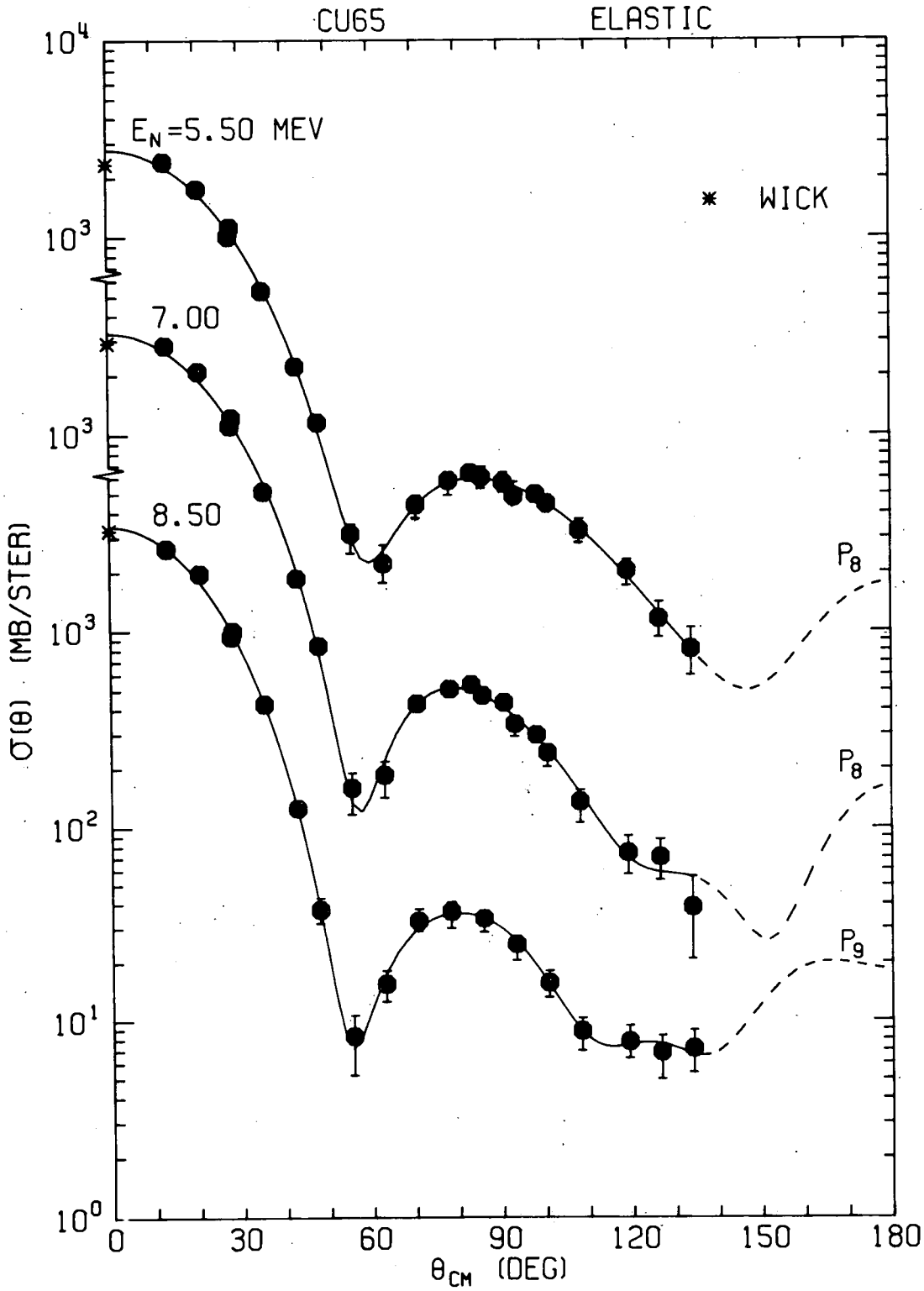

Fig. 3. Our ^{65}Cu neutron differential elastic center-of-mass scattering cross sections with Legendre fits to the data. WICK indicates Wick's Limit which was used in the fitting. The 7% uncertainty in absolute normalization common to all points is not included in the error bars.

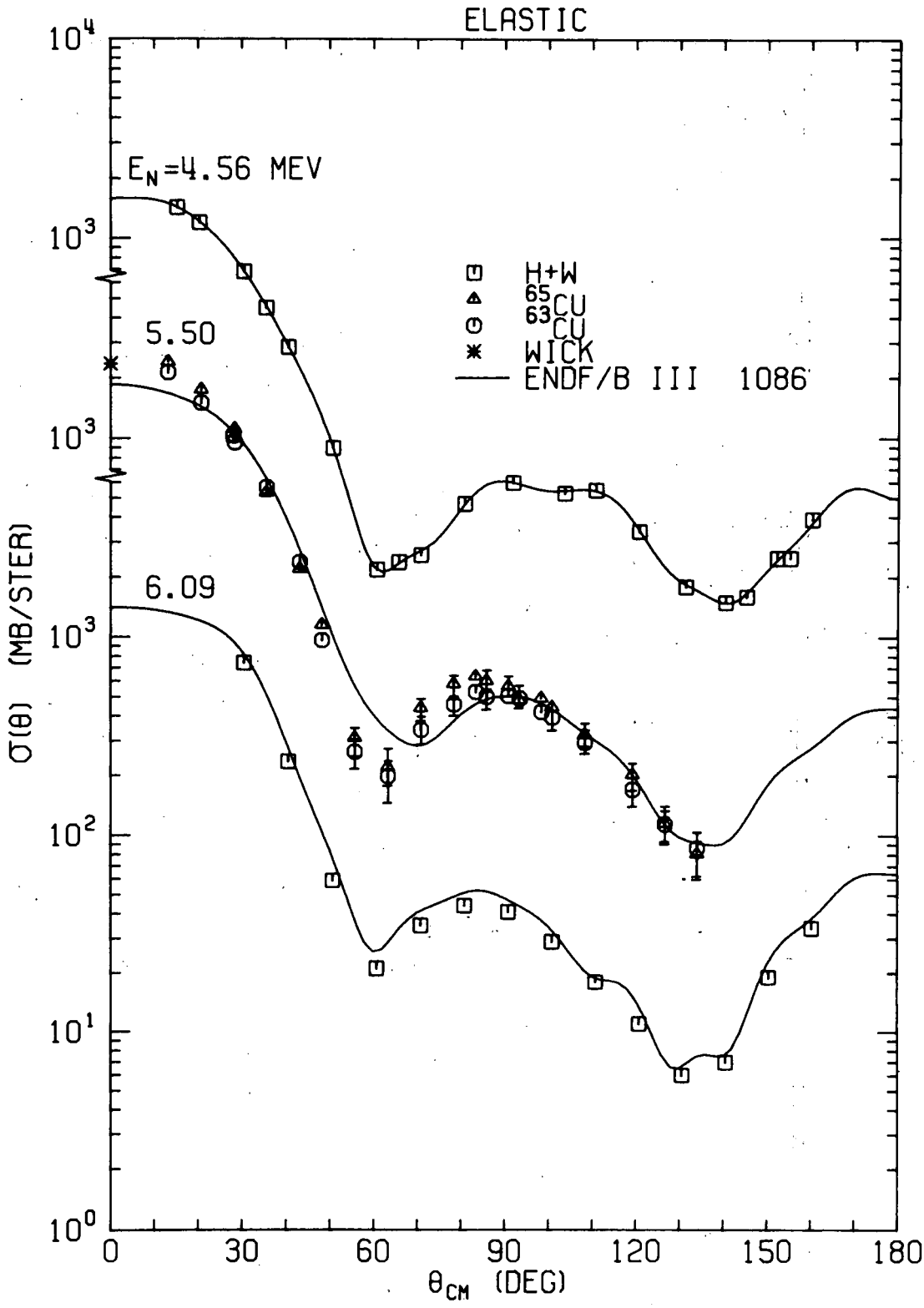

Fig. 4. Our ^{63}Cu and ^{65}Cu neutron differential elastic center-of-mass scattering cross sections compared with the data of Holmqvist and Wiedling[2] (H+W) and with ENDF/B III MAT 1086.

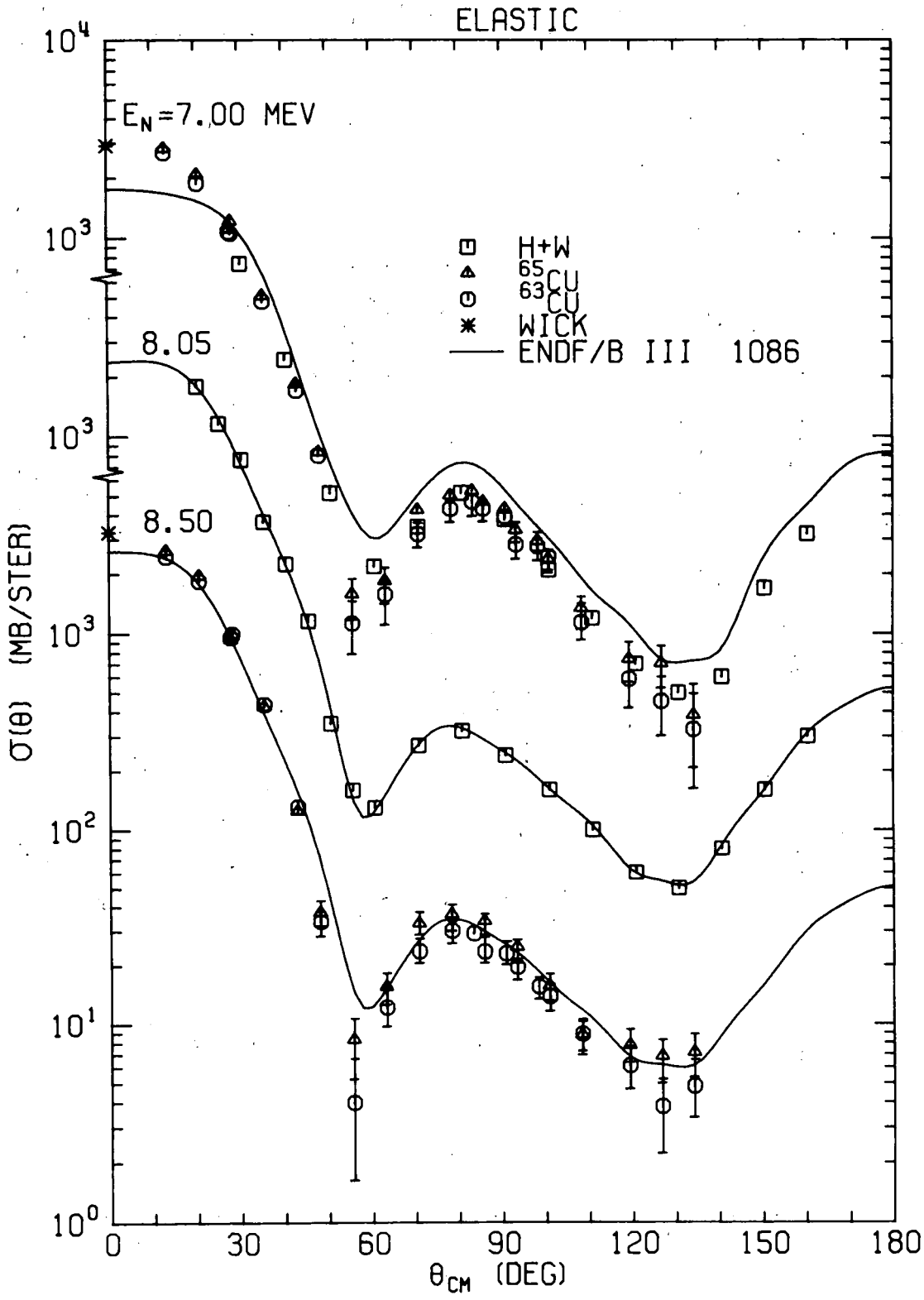

Fig. 5. Our ^{63}Cu and ^{65}Cu neutron differential elastic center-of-mass scattering cross sections compared with the data of Holmqvist and Wiedling[2] (H+W) and with ENDF/B III MAT 1086.

Holmqvist and Wiedling at 7.05 ± 0.09 MeV within experimental uncertainties and appear to agree qualitatively in shape at other energies.

The ENDF/B III MAT 1086 angular distributions were based on the results of Holmqvist and Wiedling hence are in good agreement with their results. The use of a Legendre expansion of order 20 is open to serious question in that variations in the data attributable to experimental uncertainties are faithfully reproduced in the ENDF/B description and lead to spurious structure. An expansion of order 9 is the most required to fit the experimental data adequately. The ENDF/B forward peaks are underestimated and, where it is shown, fall below Wick's Limit – at 7 MeV by a factor of 2.

Our differential elastic data might more quantitatively be compared with that of Holmqvist and Wiedling with the help of Figures 6 and 7 where the normalized Legendre expansion coefficients resulting from fits to our ^{63}Cu and ^{65}Cu data and to the data of Holmqvist and Wiedling are plotted as a function of incident neutron energy. The curves result from quadratic least squares fits to our ^{63}Cu and ^{65}Cu coefficients with constants given in the equations. Our coefficients are systematically higher than those resulting from fits to the data of Holmqvist and Wiedling. Higher coefficients imply more structure, e.g. a larger ratio of second maximum to first minimum, and this is the case upon closer inspection of Figures 4 and 5.

Inelastic Scattering Differential Cross Sections

Our differential cross sections for combined inelastic scattering to the 1.327, 1.412, and 1.547 MeV levels in ^{63}Cu are shown in Figure 8 and are isotropic within experimental uncertainties.

Our differential cross sections for inelastic scattering to the 1.115 MeV level in ^{65}Cu at an incident neutron energy of 5.50 MeV and the combined inelastic scattering to the 1.481, 1.620, and 1.720 MeV levels in ^{65}Cu at incident neutron energies from 5.50 to 8.50 MeV are shown in Figure 9. Within experimental uncertainties these also are isotropic.

Excitation Functions

Our angle-integrated differential cross sections for ^{63}Cu and ^{65}Cu are shown as a function of energy in Figure 10 along with the elastic data of Holmqvist and Wiedling[2] and the curve from ENDF/B III MAT 1086.

The systematic difference among our data and that of Holmqvist and Wiedling above 5 MeV seen in comparisons of elastic data for other elements[1] is also seen here. While the data agree above 8 MeV in this case, the average of our 7 MeV ^{63}Cu and ^{65}Cu data is higher by 506 mb, 28%, than the result of Holmqvist and Wiedling at 7.05 MeV. The average of our ^{63}Cu and ^{65}Cu data at 5.50 MeV is higher by 403 mb than the value obtained by linearly interpolating to 5.50 MeV the results of Holmqvist and Wiedling at 4.56 and 6.09 MeV.

The ENDF/B III MAT 1086 curve is in good agreement with our data. Even though ENDF/B MAT 1086 based its angular distributions on the data of Holmqvist and Wiedling between 1.46 and 8 mev, ENDF/B evaluations commonly obtain their integrated elastic scattering cross sections from the differencebetween the total and non-elastic cross sections in this energy region.

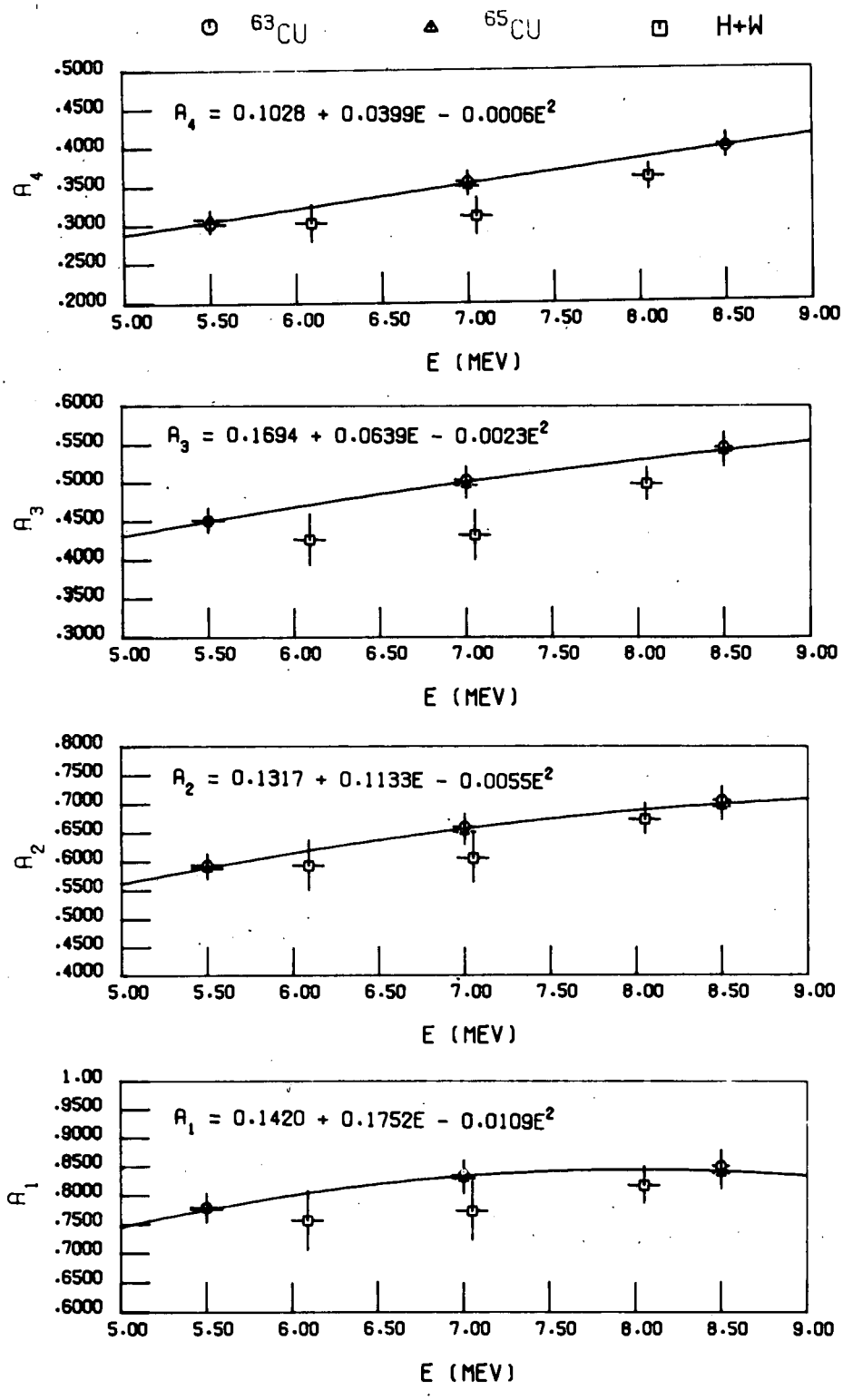

Fig. 6. The first through fourth normalized Legendre expansion coefficients obtained from fitting our ^{63}Cu and ^{65}Cu elastic differential cross sections and the data of Holmqvist and Wiedling[2] (H+W). The curves are quadratic least squares fits to our data with constants given in the equations.

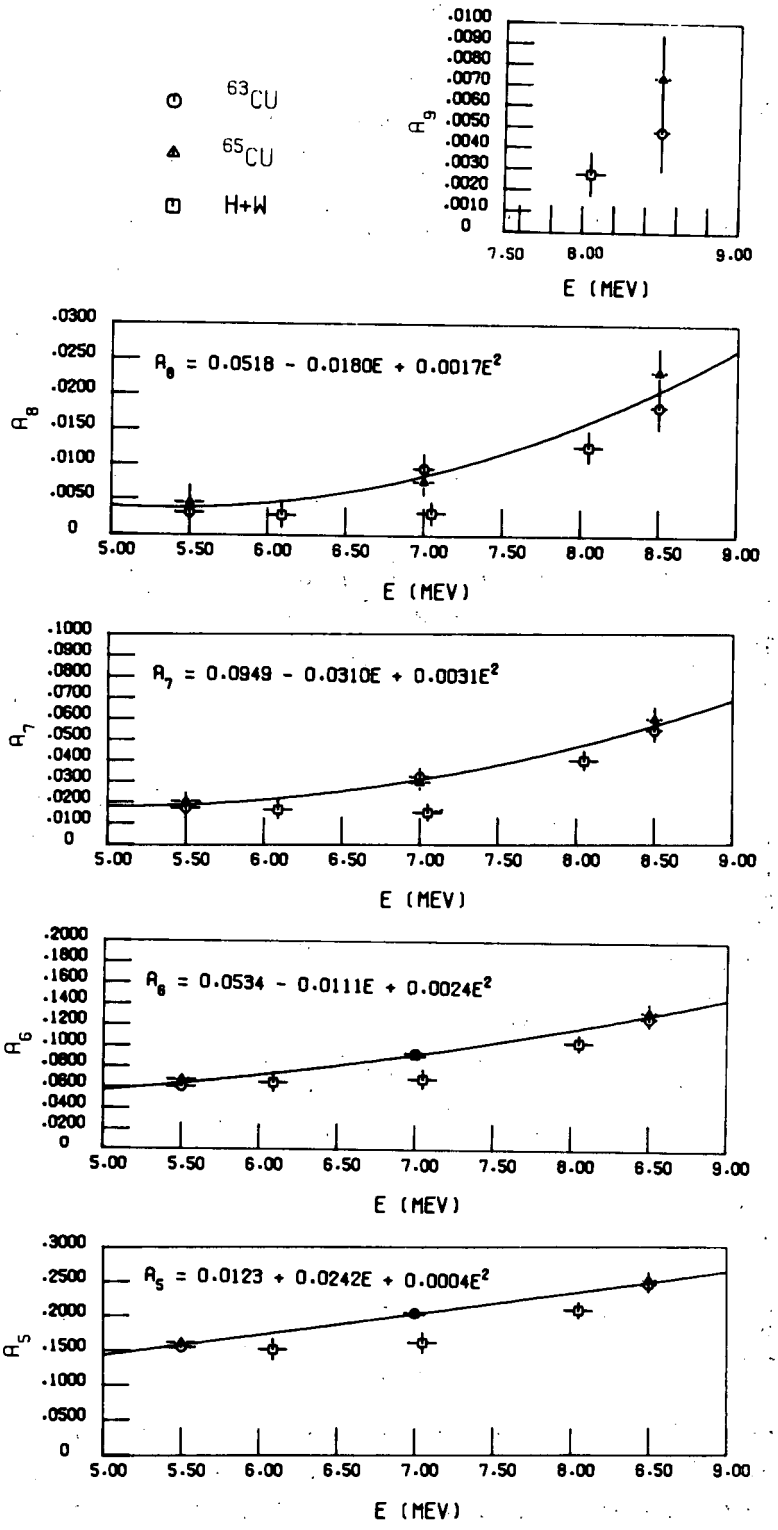

Fig. 7. The fifth through ninth normalized Legendre expansion coefficients obtained from fitting our ^{63}Cu and ^{65}Cu elastic differential cross sections and the data of Holmqvist and Wiedling[2] (H+W). The curves are quadratic least squares fits to our data with constants given in the equations.

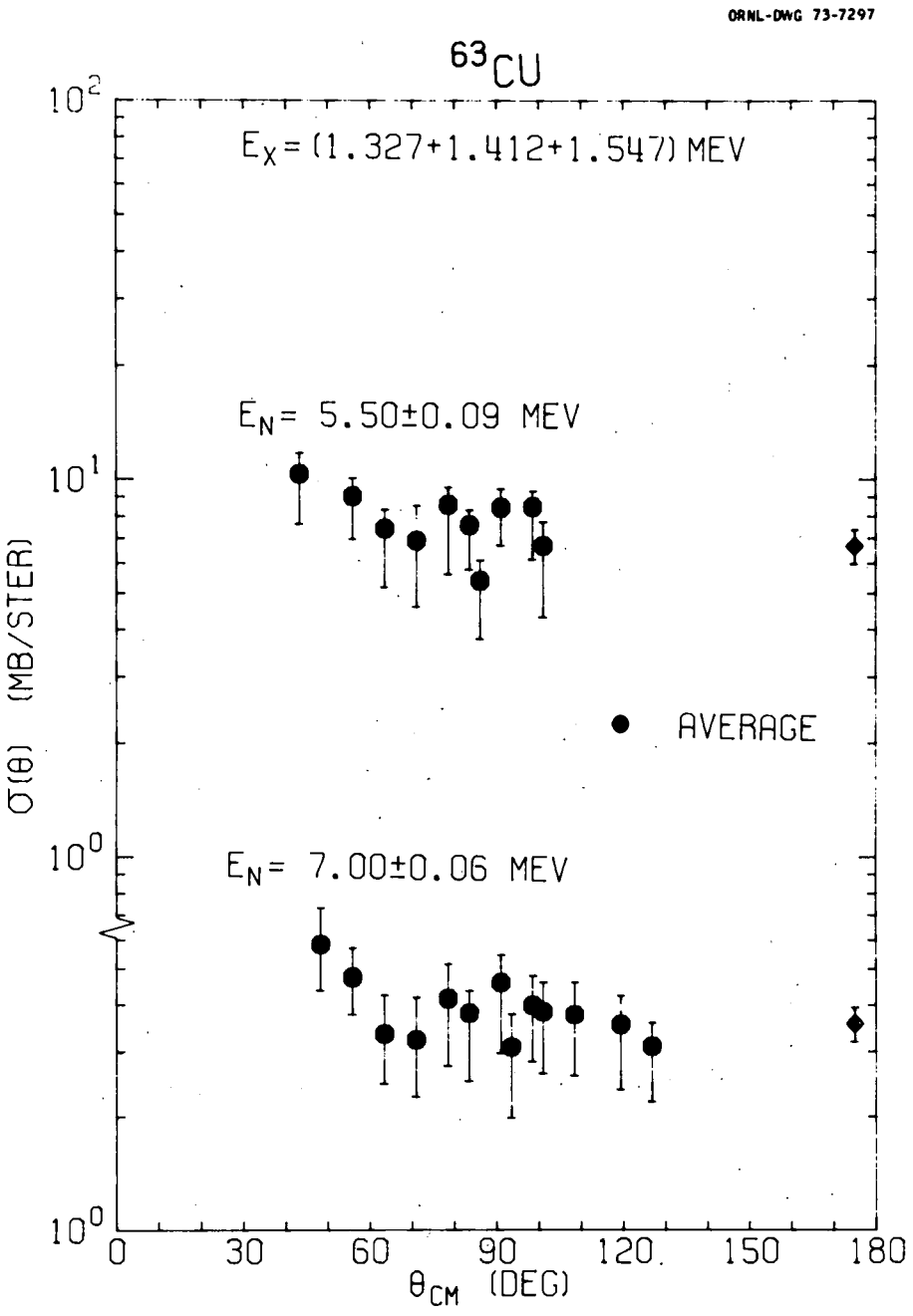

Fig. 8. Our ^{63}Cu neutron differential center-of-mass cross sections for combined inelastic scattering to the 1.327, 1.412, and 1.547 MeV levels in ^{63}Cu. The 7% uncertainty in absolute normalization common to all points is not included in the error bars.

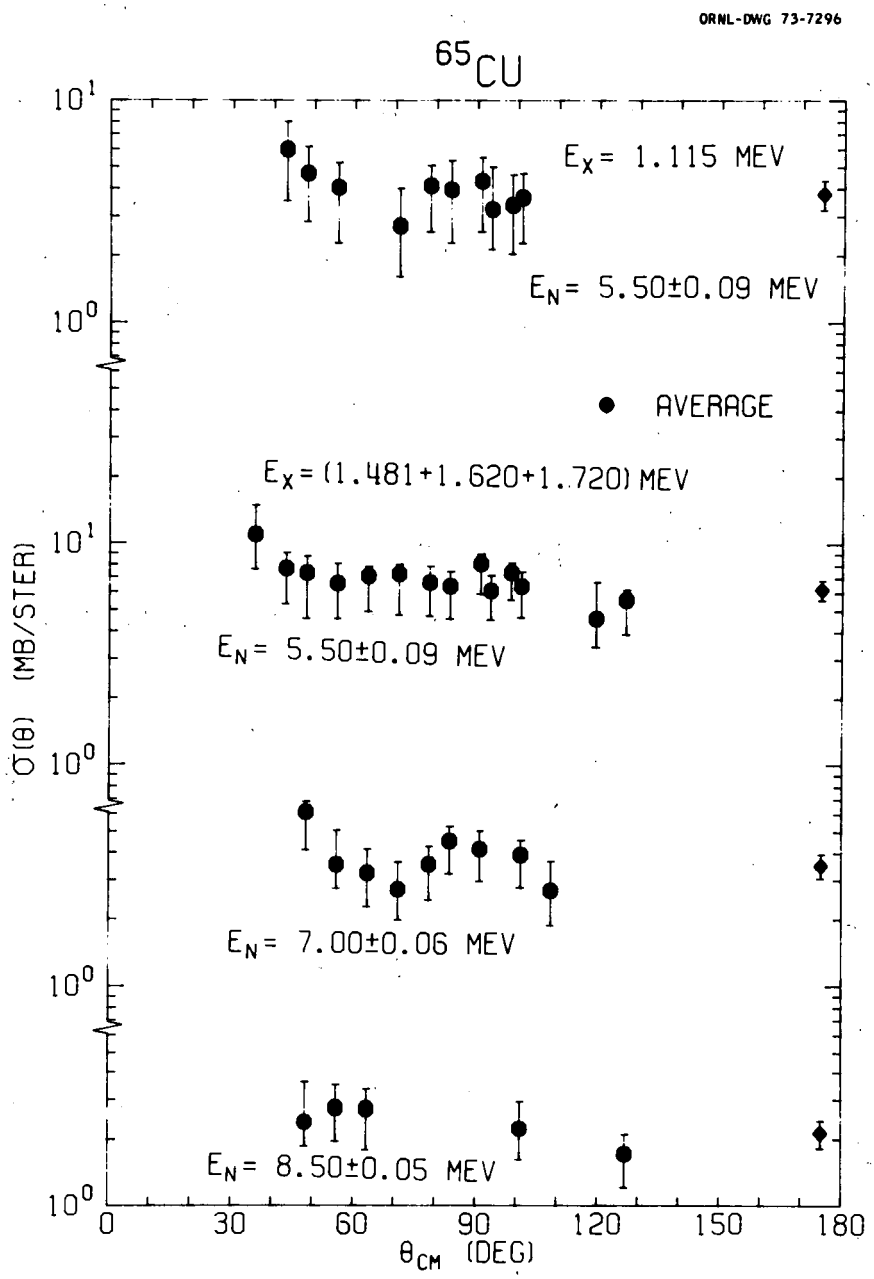

Fig. 9. Our ^{65}Cu neutron center-of-mass differential inelastic scattering cross sections. The 7% uncertainty in absolute normalization common to all points is not included in the error bars.

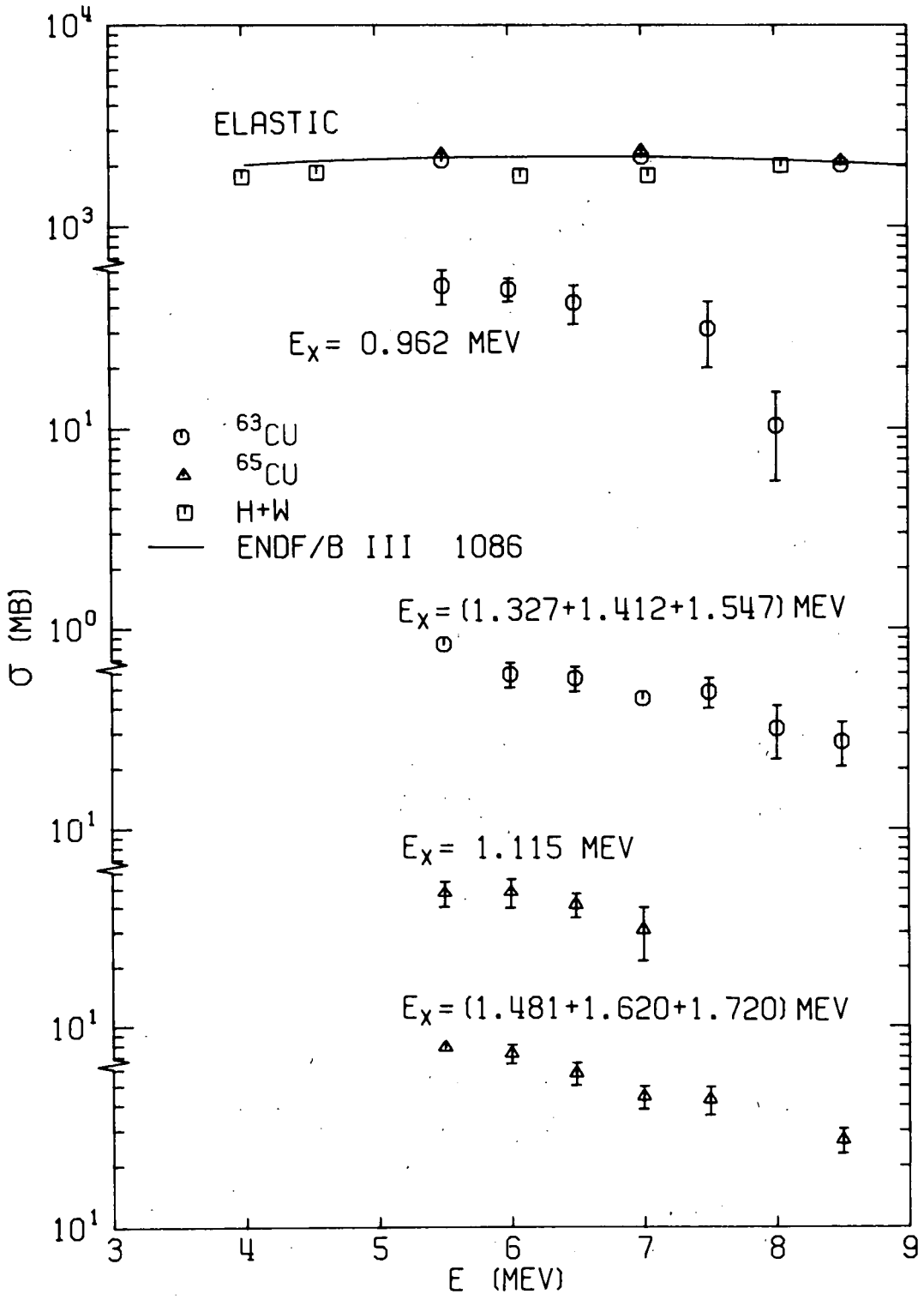

Fig. 10. Our ^{63}Cu and ^{65}Cu angle-integrated differential cross sections as a function of incident neutron energy with the elastic data of Holmqvist and Wiedling[2] (H+W) and the curve from ENDF/B III MAT 1086. The 7% uncertainty in absolute normalization is included in our error bars.

ENDF/B III MAT 1085 and 1086 describe all inelastic scattering above an incident neutron energy of 1.75 MeV as continuum inelastic scattering.

Inelastic Scattering to the Continuum

At excitation energies above 1.55 MeV in ^{63}Cu and 1.72 MeV in ^{65}Cu we treated inelastic scattering as scattering to a continuum rather than attempting to extract cross sections for inelastic scattering to groups of levels or bands of excitation energy. Figures 11 and 12 show our angle-averaged double-differential cross sections for scattering to an excitation energy as a function of excitation energy for ^{63}Cu and ^{65}Cu, respectively. The differences in resolution at which the measurements were made at various energies is readily apparent, underscoring the fact that what is called a continuum is very much a matter of resolution. Both isotopes display structure but not nearly to the extent that the even-even isotopes have shown in our other work.[1]

The success one might expect in applying an evaporation model to the copper isotopes may be judged from Figures 13 through 16 where SIG(E → E′)/E′ is plotted versus E′ with SIG(E → E′) = our angle-averaged cross section for inelastic scattering from incident energy E to outgoing energy dE′ about E′. The fits have been made to an excitation energy of roughly 3.5 MeV for both ^{63}Cu and ^{65}Cu. The straight lines are least squares fits to the logarithms of the data with resulting temperatures and their fitting uncertainties given. Again, the adequacy of an evaporation model depends on the resolution at which the data were taken. In this case, an evaporation model would seem to offer an adequate description of continuum inelastic scattering to levels as low as 3.5 MeV excitation energy in the residual nucleus. Note that the temperatures increase from about 0.8 MeV at an incident neutron energy of 5.5 MeV to a value of roughly 1.05 MeV at an incident energy of 8.5 MeV.

ENDF/B III MAT 1085 and 1086 describe all inelastic scattering above an incident neutron energy of 1.75 MeV as inelastic scattering to a continuum and use an evaporation model with a constant temperature of 1 MeV.

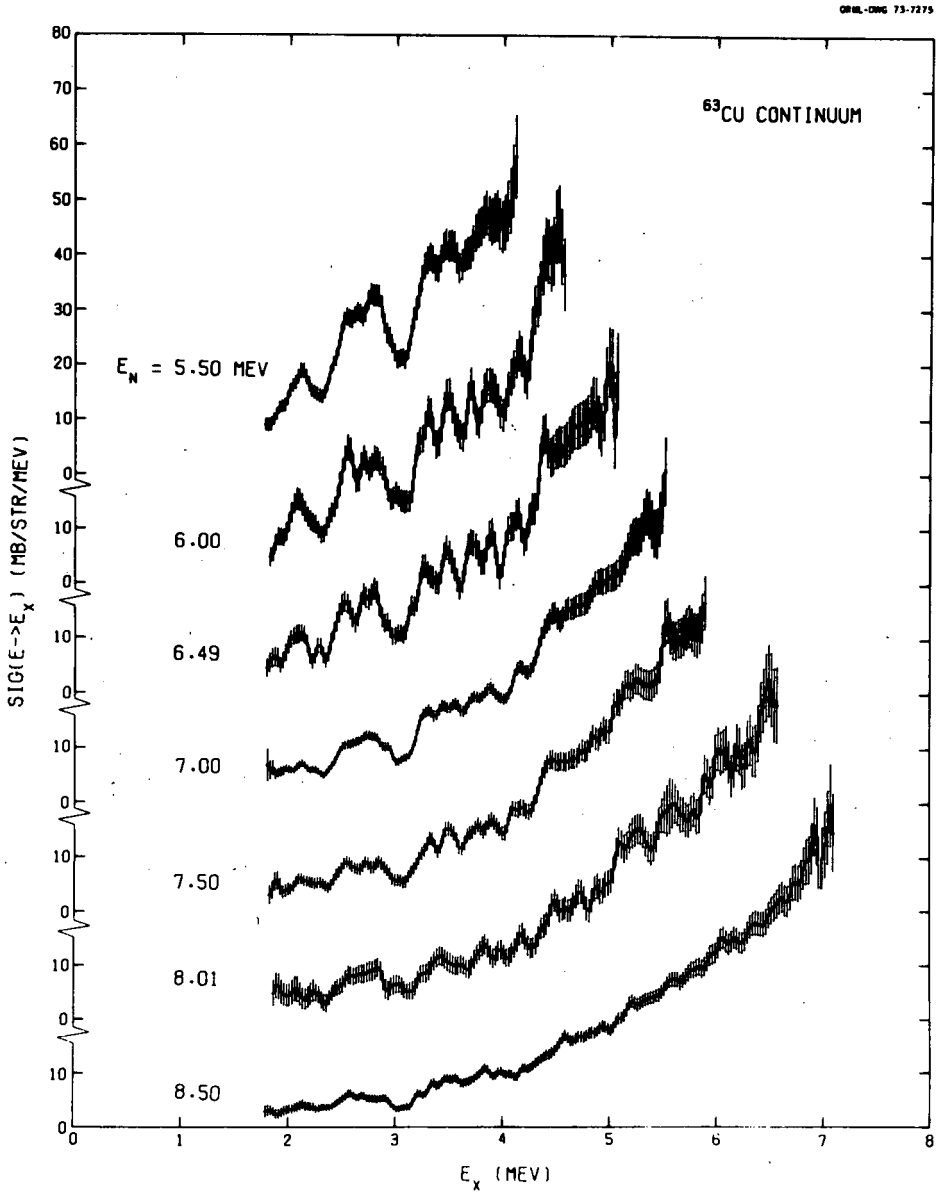

Fig. 11. Our ^{63}Cu angle-averaged double-differential cross sections for scattering from an incident neutron energy E to an excitation energy as a function of excitation energy.

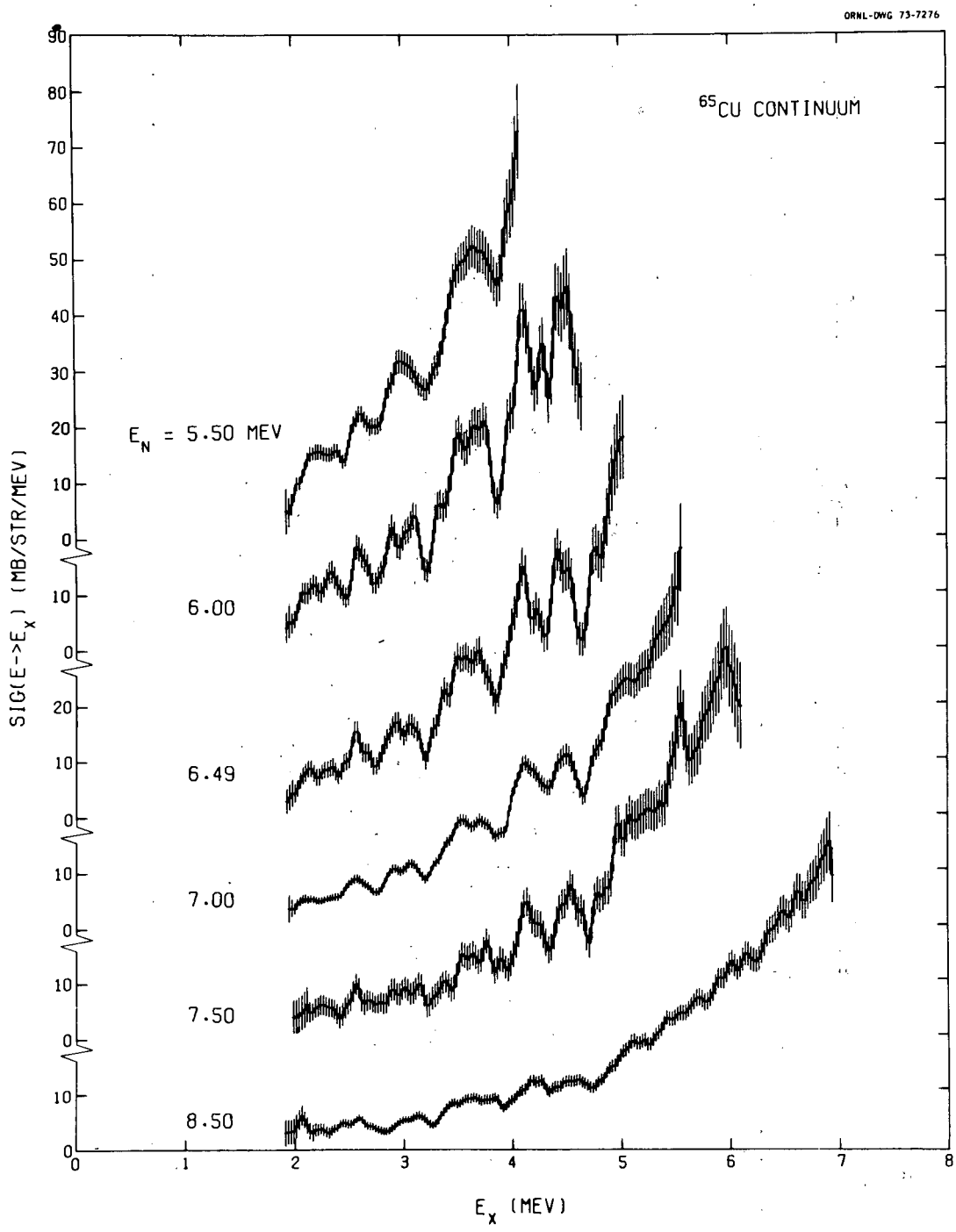

Fig. 12. Our ^{65}Cu angle-averaged double-differential cross sections for scattering from an incident neutron energy E to an excitation energy as a function of excitation energy.

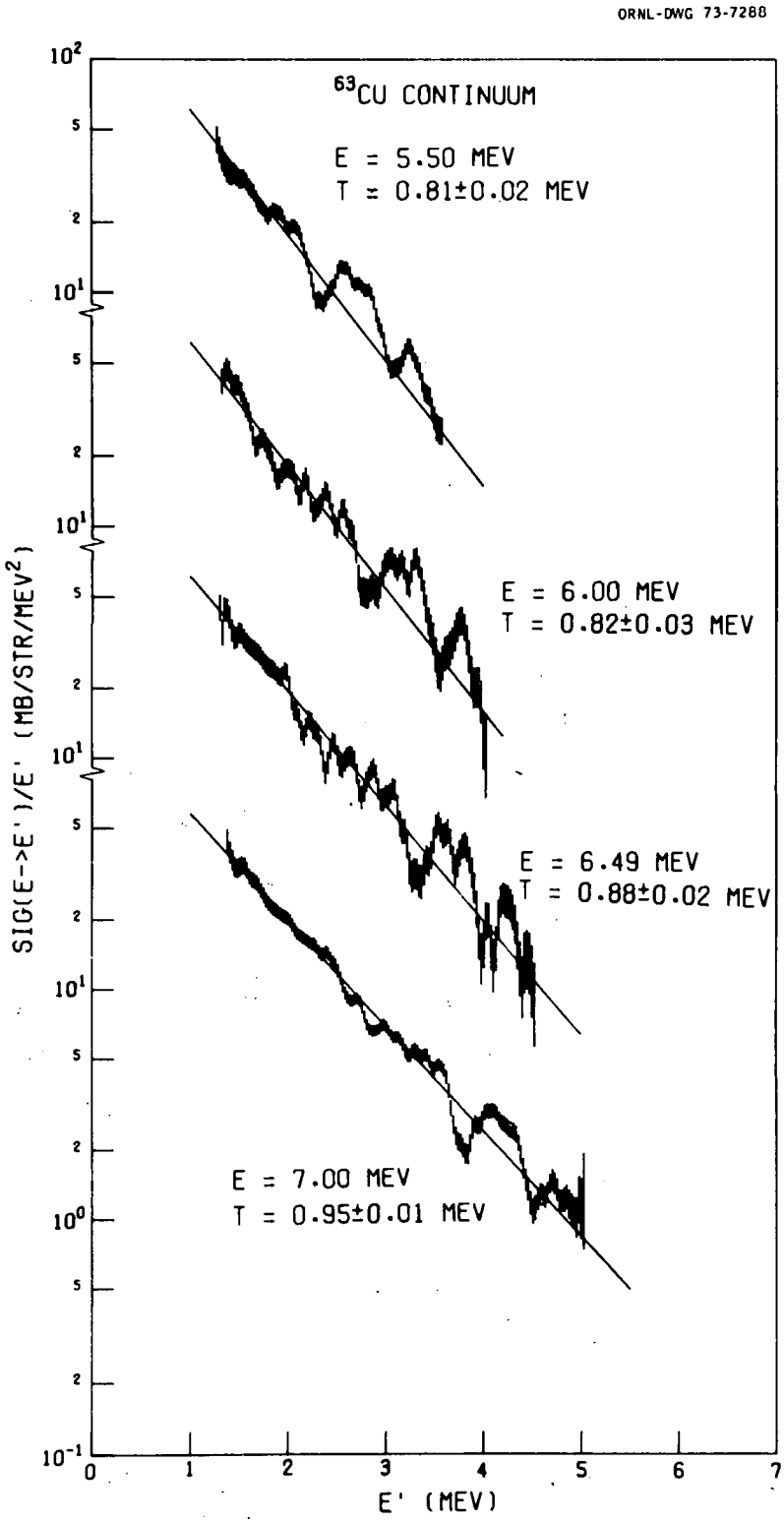

Fig. 13. Our ^{63}Cu angle-averaged double-differential cross sections for scattering from incident neutron energy E to outgoing neutron energy dE′ about E′ divided by E′ as a function of E′. The straight lines are least squares fits to the data corresponding to excitation energy $>$ 3.5 MeV with resulting temperatures indicated. The uncertainties on the temperatures are fitting uncertainties only.

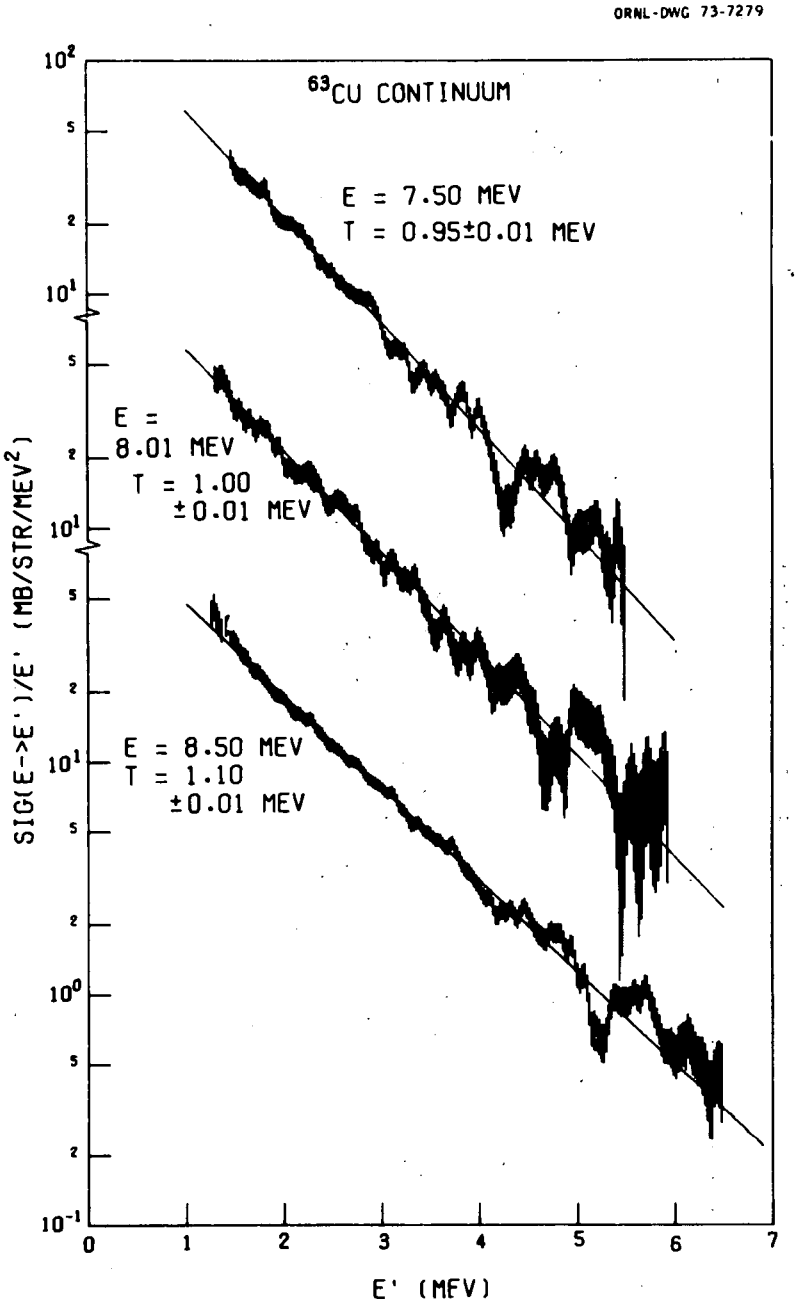

Fig. 14. Our ^{63}Cu angle-averaged double-differential cross sections for scattering from incident neutron energy, E, to outgoing neutron energy dE′ about E′ divided by E′ as a function of E′. The straight lines are least squares fits to the data corresponding to excitation energy $>$ 3.5 MeV with resulting temperatures indicated. The uncertainties on the temperatures are fitting uncertainties only.

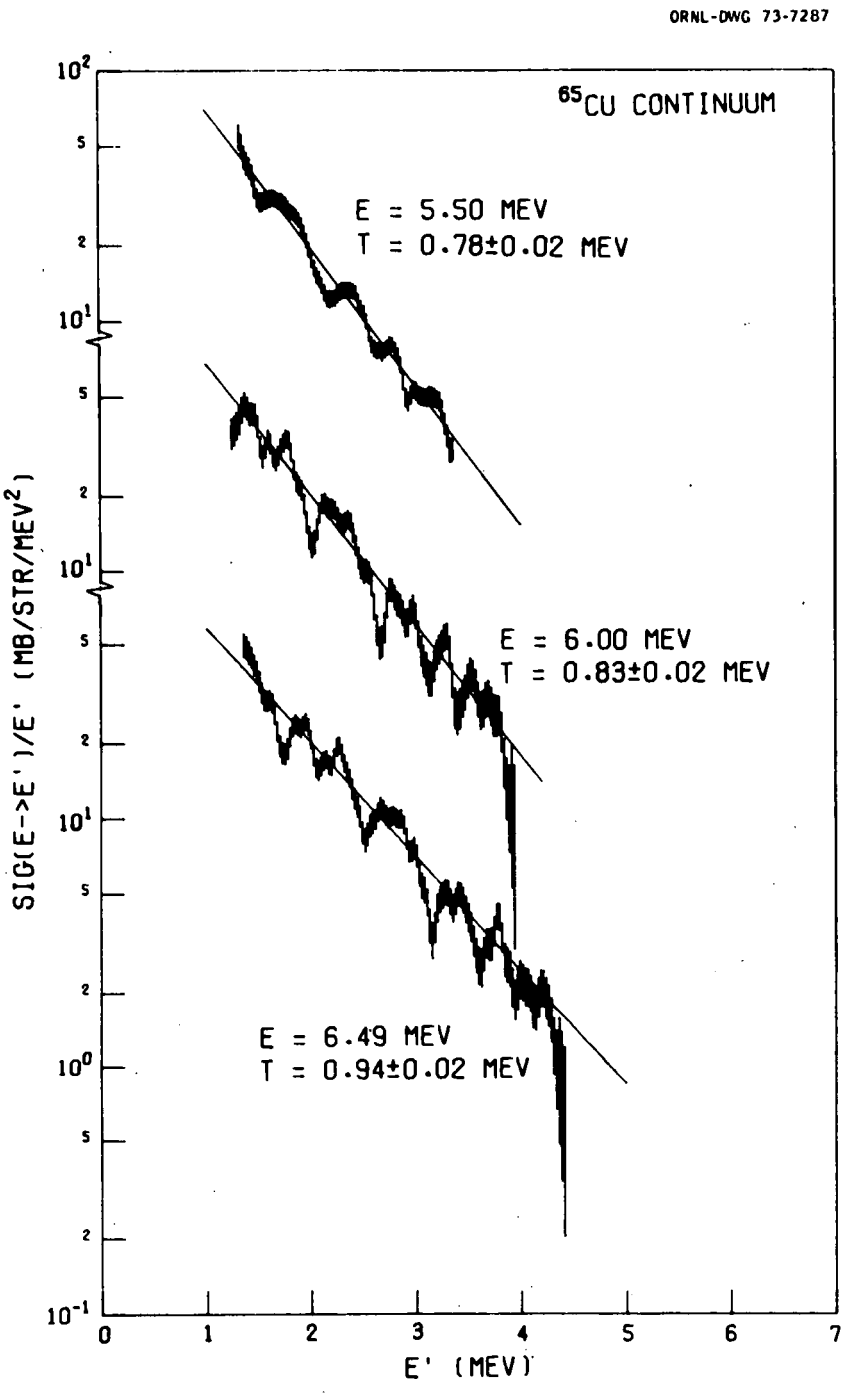

Fig. 15. Our ^{65}Cu angle-averaged double-differential cross sections for scattering from incident neutron energy E to outgoing neutron energy dE′ about E′ divided by E′ as a function of E′. The straight lines are least squares fits to the data corresponding to excitation energy $>$ 3.5 MeV with resulting temperatures indicated. The uncertainties on the temperatures are fitting uncertainties only.

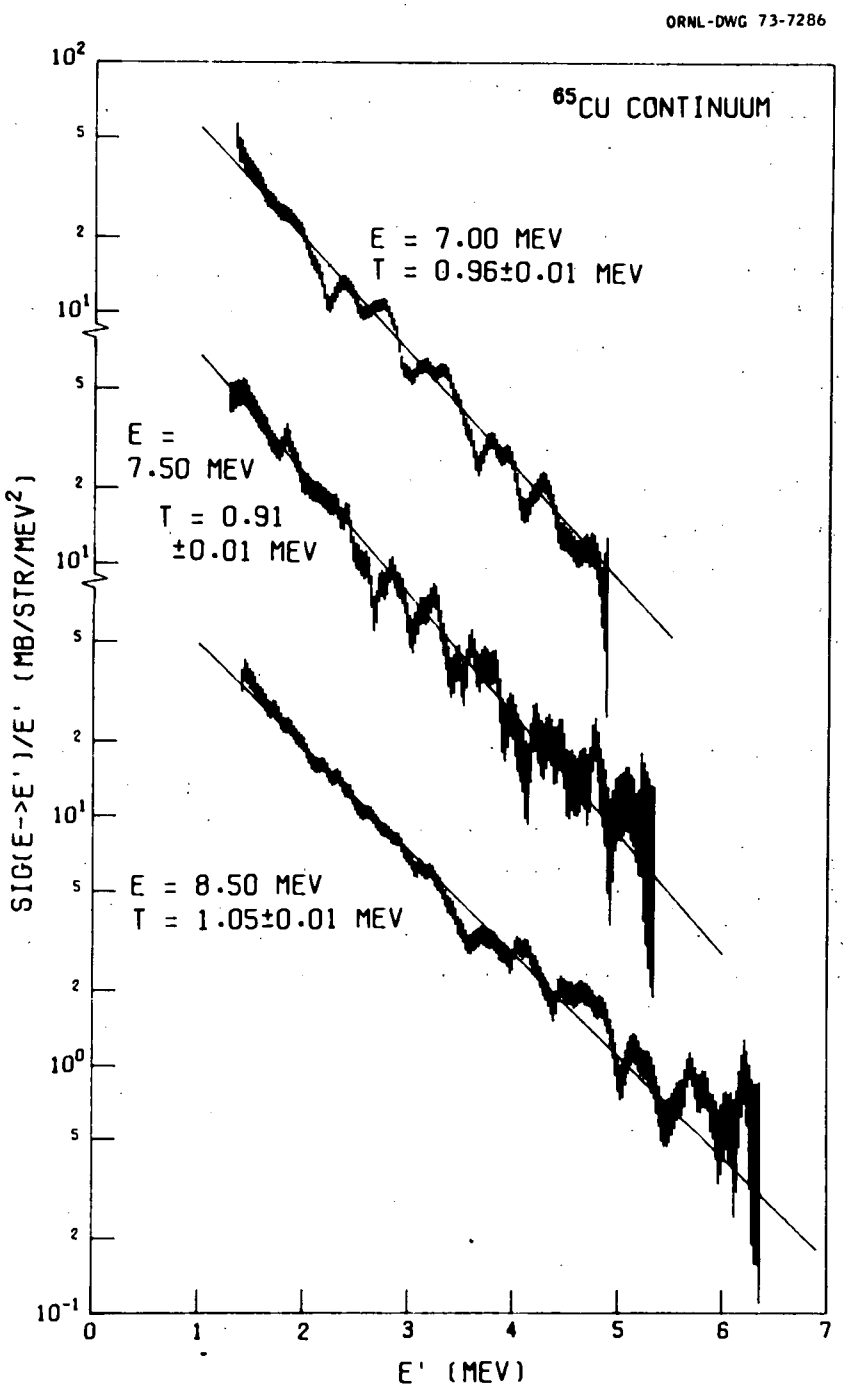

Fig. 16. Our ^{65}Cu angle-averaged double-differential cross sections for scattering from incident neutron energy E to outgoing neutron energy dE′ about E′ divided by E′ as a function of E′. The straight lines are least squares fits to the data corresponding to excitation energy $>$ 3.5 MeV with resulting temperatures indicated. The uncertainties on the temperatures are fitting uncertainties only.

CONCLUSIONS

Our ^{63}Cu and ^{65}Cu differential elastic scattering cross sections are in good agreement both in shape and magnitude. These data are in fair agreement with the natural copper elastic data of Holmqvist and Wiedling. Our differential cross sections show somewhat more structure than do theirs. The systematic differences among our angle-integrated differential elastic data and the integrals of the data of Holmqvist and Wiedling above 5 MeV which occur in comparisons of the two data sets for other elements are also present here, our data being higher by 28% at 7 MeV. ENDF/B III MAT 1085 and 1086 elastic angular distributions when normalized to experimental integrals underestimate the forward peak at angles less than 20 deg. and introduce unphysical fluctuations through the use of a Legendre series of order 20.

An evaporation model of inelastic scattering to the continuum offers a reasonable description for inelastic scattering to levels above an excitation energy of 3.5 MeV in the residual nucleus. Nuclear temperatures rise from a value of 0.8 MeV at an incident neutron energy of 5.5 MeV to a value of 1.05 MeV at an incident energy of 8.5 MeV.

ACKNOWLEDGMENTS

Many have contributed to this experimental program at one time or another and we would like to thank them for their contributions. In particular, we would like to acknowledge the help of J. K. Dickens, J. W. McConnell, J. A. Biggerstaff, A. M. Marusak, P. H. Stelson, C. O. LeRigoleur, and E. Hungerford.

We are deeply indebted to F. C. Maienschein, director of the Neutron Physics Division, for his support of the experiment with the use of computers in report preparation and type setting which produced this report and the other six of our last seven reports.

REFERENCES

1. F. G. Perey and W. E. Kinney, "Carbon Neutron Elastic- and Inelastic-Scattering Cross Sections from 4.5 to 8.5 MeV", ORNL-4441 (December 1970).

F. G. Perey, C. O. LeRigoleur and W. E. Kinney, "Nickel-60 Neutron Elastic- and Inelastic-Scattering Cross Sections from 6.5 to 8.5 MeV", ORNL-4523 (April 1970).

W. E. Kinney and F. G. Perey, "Neutron Elastic- and Inelastic-Scattering Cross Sections from ^{56}Fe in the Energy Range 4.19 to 8.56 MeV", ORNL-4515 (June 1970).

F. G. Perey and W. E. Kinney, "Calcium Neutron Elastic- and Inelastic-Scattering Cross Sections from 4.0 to 8.5 MeV", ORNL-4519 (April 1970).

F. G. Perey and W. E. Kinney, "Sulfur Neutron Elastic- and Inelastic-Scattering Cross Sections from 4 to 8.5 MeV", ORNL-4539 (June 1970).

W. E. Kinney and F. G. Perey, "Neutron Elastic- and Inelastic- Scattering Cross Sections for Co in the Energy Range 4.19 to 8.56 MeV", ORNL-4549 (June 1970).

W. E. Kinney and F. G. Perey, "Neutron Elastic- and Inelastic- Scattering Cross Sections for Mg in the Energy Range 4.19 to 8.56 MeV", ORNL-4550 (June 1970).

W. E. Kinney and F. G. Perey, "Neutron Elastic- and Inelastic- Scattering Cross Sections for Si in the Energy Range 4.19 to 8.56 MeV", ORNL-4517 (July 1970).

F. G. Perey and W. E. Kinney, "Neutron Elastic and Inelastic- Scattering Cross Sections for Na in the Energy Range of 5.4 to 8.5 MeV", ORNL-4518 (August 1970).

W. E. Kinney and F. G. Perey, "Al Neutron Elastic- and Inelastic- Scattering Cross Sections from 4.19 to 8.56 MeV", ORNL-4516 (October 1970).

F. G. Perey and W. E. Kinney, "V Neutron Elastic- and Inelastic- Scattering Cross Sections from 4.19 to 8.56 MeV", ORNL-4551 (October 1970).

F. G. Perey and W. E. Kinney, "Neutron Elastic- and Inelastic- Scattering Cross Sections for Yttrium in the Energy Range 4.19 to 8.56 MeV", ORNL-4552 (December 1970).

W. E. Kinney and F. G. Perey, "Neutron Elastic- and Inelastic- Scattering Cross Sections for Oxygen in the Energy Range 4.34 to 8.56 MeV", ORNL-4780 (April 1972).

W. E. Kinney and F. G. Perey, "W Neutron Elastic- and Inelastic- Scattering Cross Sections from 4.34 to 8.56 MeV", ORNL-4803 (May 1973).

W. E. Kinney and F. G. Perey, "^{238}U Neutron Elastic-Scattering Cross Sections from 6.44 to 8.56 MeV", ORNL-4804 (June 1973).

W. E. Kinney and F. G. Perey, "Natural Titanium Neutron Elastic and Inelastic Scattering Cross Sections from 4.07 to 8.56 MeV", ORNL-4810 (October 1973).

W. E. Kinney and F. G. Perey, "Natural Nickel and ^{60}Ni Neutron Elastic and Inelastic Scattering Cross Sections from 4.07 to 8.56 MeV", ORNL-4807 (November 1973).

W. E. Kinney and F. G. Perey, "Natural Chromium and ^{52}Cr Neutron Elastic and Inelastic Scattering Cross Sections from 4.07 to 8.56 MeV", ORNL-4806 (November 1973).

F. G. Perey and W. E. Kinney, "Nitrogen Neutron Elastic and Inelastic Scattering Cross Sections from 4.34 to 8.56 MeV", ORNL-4805 (January 1974).

W. E. Kinney and F. G. Perey, "^{54}Fe Neutron Elastic and Inelastic Scattering Cross Sections from 4.34 to 8.56 MeV", ORNL-4907 (January 1974).

W. E. Kinney and F. G. Perey, "^{206}Pb, ^{207}Pb, and ^{208}Pb Neutron Elastic and Inelastic Scattering Cross Sections from 5.50 to 8.50 MeV", ORNL-4909 (To be published).

2. B. Holmqvist and T. Wiedling, "Neutron Elastic Scattering Cross Sections, Experimental Data and Optical Model Calculations", AE-366, Aktiebolaget Atomenergi (1969).

3. W. E. Kinney, "Neutron Elastic and Inelastic Scattering from ^{56}Fe from 4.60 to 7.55 MeV", ORNL-TM-2052, (January 1968).

4. R. E. Textor and V. V. Verbinski, "05S: A Monte Carlo Code for Calculating Pulse Height Distributions Due to Monoenergetic Neutrons Incident on Organic Scintillators", ORNL-4160 (February 1968).

APPENDIX

Tabulated Values of ^{63}Cu and ^{65}Cu Neutron Elastic Scattering Cross Sections and Cross Sections for Inelastic Scattering to Discrete Levels

Our measured values for ^{63}Cu and ^{65}Cu neutron elastic scattering and cross sections for inelastic scattering to discrete levels are tabulated below. The uncertainties in differential cross sections, indicated by Δ in the tables, are relative and do *not* include a $\pm 7\%$ uncertainty in detector efficiency which is common to all points. The $\pm 7\%$ uncertainty is included in the integrated and average values. The total cross sections, T, are those we used in the computation of Wick's Limit and were not measured by us.

We have not included the cross sections for inelastic scattering to the continuum. They are available from the National Neutron Cross Section Center, Brookhaven National Laboratory, or from us.

^{63}Cu cross sections may be found on pages 26 through 29. ^{65}Cu cross sections may be found on pages 30 through 33.

^{63}Cu CROSS SECTIONS

$E_n = 5.50 \pm 0.09$ MeV
Elastic Scattering

θ_{cm}	$d\sigma/d\omega$	Δ (%)	
deg.	*mb/str*	+	−
13.10	2136.28	4.8	4.8
20.70	1505.76	6.2	5.3
27.93	1038.49	4.6	5.6
28.30	957.21	6.7	5.1
35.53	570.27	5.3	5.8
43.12	239.07	5.2	7.2
48.18	96.60	9.1	7.3
55.75	26.45	15.8	18.2
63.31	19.83	20.0	26.4
70.86	34.39	16.0	16.0
78.39	46.15	9.4	12.4
83.41	53.30	7.5	8.8
85.91	50.24	9.2	13.6
90.91	50.84	7.2	9.7
93.42	49.42	7.4	13.2
98.41	42.31	6.8	11.5
100.90	39.80	7.7	14.2
108.38	29.47	16.0	12.1
119.31	17.04	15.1	17.9
126.74	11.41	17.0	20.7
134.17	8.63	20.7	27.9

$\int(d\sigma/d\omega)d\omega$ = 2125.28 mb ± 7.5 %
Wick's Limit = 2351.97 mb ± 9.2 %
σ_T = 3.80 b ± 3.0 %

Legendre Fit, Order = 8

k	a_k	Δ(%)
0	338.24878	2.0
1	263.57153	2.3
2	200.75175	2.6
3	152.51503	2.8
4	101.93570	3.2
5	52.20876	4.9
6	20.54915	9.2
7	5.87353	21.5
8	1.05246	74.8

$E_n = 5.50 \pm 0.09$ MeV
(n,n′) to: 0.962 MeV Level

θ_{cm}	$d\sigma/d\omega$	Δ (%)	
deg.	*mb/str*	+	−
63.40	3.32	30.5	30.5
83.50	4.60	14.0	25.8
91.01	5.16	10.2	36.0

Avg. $d\sigma/d\omega$ = 4.05 mb/str ± 19.2%
$\int(d\sigma/d\omega)d\omega$ = 50.92 mb ± 19.2 %

$E_n = 5.50 \pm 0.09$ MeV
(n,n′) to: 1.327 MeV Level
+ 1.412 MeV Level
+ 1.547 MeV Level

θ_{cm}	$d\sigma/d\omega$	Δ (%)	
deg.	*mb/str*	+	−
43.22	10.33	13.5	26.2
55.87	9.03	11.4	23.0
63.44	7.42	12.1	30.2
71.00	6.90	23.5	33.5
78.53	8.58	11.0	34.6
83.55	7.58	9.6	23.9
86.06	5.40	13.2	30.2
91.06	8.42	11.8	20.6
98.55	8.46	9.8	27.5
101.05	6.68	15.6	35.5

Avg. $d\sigma/d\omega$ = 6.67 mb/str ± 10.5%
$\int(d\sigma/d\omega)d\omega$ = 83.80 mb ± 10.5 %

$E_n = 6.00 \pm 0.04$ MeV
(n,n′) to: 0.962 MeV Level

θ_{cm}	$d\sigma/d\omega$	Δ (%)	
deg.	*mb/str*	+	−
83.49	3.81	11.9	34.7
91.00	4.38	14.2	31.7
98.49	4.22	14.1	31.6

Avg. $d\sigma/d\omega$ = 3.89 mb/str ± 12.9%
$\int(d\sigma/d\omega)d\omega$ = 48.89 mb ± 12.9 %

$E_n = 6.00 \pm 0.04$ MeV
(n,n′) to: 1.327 MeV Level
+ 1.412 MeV Level
+ 1.547 MeV Level

θ_{cm}	$d\sigma/d\omega$	Δ (%)	
deg.	*mb/str*	+	−
83.53	4.71	14.7	24.0
91.04	6.22	11.2	23.4
98.53	4.36	16.4	24.1

Avg. $d\sigma/d\omega$ = 4.71 mb/str ± 14.1 %
$\int(d\sigma/d\omega)d\omega$ = 59.19 mb ± 14.1 %

$E_n = 6.49 \pm 0.04$ MeV
(n,n′) to: 0.962 MeV Level

θ_{cm}	$d\sigma/d\omega$	Δ (%)	
deg.	*mb/str*	+	−
83.48	2.49	41.3	35.1
90.99	3.67	19.0	33.2
98.48	4.29	13.2	30.1

Avg. $d\sigma/d\omega$ = 3.33 mb/str ± 21.6 %
$\int(d\sigma/d\omega)d\omega$ = 41.91 mb ± 21.6 %

$E_n = 6.49 \pm 0.04$ MeV
(n,n′) to: 1.327 MeV Level
+ 1.412 MeV Level
+ 1.547 MeV Level

θ_{cm}	$d\sigma/d\omega$	Δ (%)	
deg.	*mb/str*	+	−
83.52	4.40	15.3	28.1
91.03	4.45	24.1	20.9
98.52	5.01	16.4	29.3

Avg. $d\sigma/d\omega$ = 4.49 mb/str ± 14.1 %
$\int(d\sigma/d\omega)d\omega$ = 56.45 mb ± 14.1 %

$E_n = 7.00 \pm 0.06$ MeV
Elastic Scattering

θ_{cm}	$d\sigma/d\omega$	Δ (%)	
deg.	*mb/str*	+	−
13.10	2688.82	5.5	4.6
20.70	1883.52	4.8	4.8
27.92	1073.98	5.4	6.5
28.30	1055.67	5.5	5.5
35.53	481.56	7.4	5.2
43.12	171.10	10.0	7.0
48.17	80.56	7.6	9.9
55.75	11.29	29.4	30.2
63.31	15.81	16.1	29.6
70.86	31.96	14.4	14.3
78.39	42.97	10.0	14.2
83.41	46.75	8.8	15.3
85.91	43.12	8.4	13.9
90.91	39.29	7.6	11.9
93.41	28.24	14.4	15.3
98.41	27.73	9.2	15.1
100.90	24.60	8.2	14.9
108.37	11.37	25.3	18.5
119.30	5.86	29.7	28.7
126.74	4.52	32.6	33.1
134.16	3.25	52.2	50.1

$\int(d\sigma/d\omega)d\omega$ = 2212.25 mb ± 7.3 %
Wick's Limit = 2915.16 mb ± 9.2 %
σ_T = 3.75 b ± 3.0 %

Legendre Fit, Order = 8

k	a_k	Δ(%)
0	352.09058	2.1
1	293.65063	2.3
2	232.30872	2.6
3	177.39481	2.7
4	125.08156	3.0
5	71.44493	3.9
6	32.85547	6.0
7	11.38279	10.8
8	3.32904	21.0

$E_n = 7.00 \pm 0.06$ MeV
(n,n') to: 1.327 MeV Level
+ 1.412 MeV Level
+ 1.547 MeV Level

θ_{cm}	$d\sigma/d\omega$	Δ (%)	
deg.	*mb/str*	+	−
48.26	5.85	25.2	25.2
55.83	4.75	20.6	20.6
63.41	3.35	26.8	26.8
70.96	3.23	29.9	29.9
78.49	4.17	23.4	34.1
83.51	3.81	14.5	34.6
91.02	4.59	19.1	35.4
93.52	3.09	22.7	35.8
98.51	3.99	20.2	29.4
101.01	3.84	20.0	32.0
108.47	3.77	22.2	31.7
119.40	3.55	19.3	33.4
126.82	3.10	15.4	29.4

Avg. $d\sigma/d\omega$ = 3.56 mb/str ± 10.7 %
$\int(d\sigma/d\omega)d\omega$ = 44.79 mb ± 10.7 %

$E_n = 7.50 \pm 0.03$ MeV
(n,n') to: 0.962 MeV Level

θ_{cm}	$d\sigma/d\omega$	Δ (%)	
deg.	*mb/str*	+	−
83.47	2.48	23.0	47.9

Avg. $d\sigma/d\omega$ = 2.48 mb/str ± 36.1 %
$\int(d\sigma/d\omega)d\omega$ = 31.12 mb ± 36.1 %

$E_n = 7.50 \pm 0.03$ MeV
(n,n') to: 1.327 MeV Level
+ 1.412 MeV Level
+ 1.547 MeV Level

θ_{cm}	$d\sigma/d\omega$	Δ (%)	
deg.	*mb/str*	+	−
83.50	4.15	10.1	32.1
91.01	3.77	17.4	38.1

Avg. $d\sigma/d\omega$ = 3.84 mb/str ± 17.0 %
$\int(d\sigma/d\omega)d\omega$ = 48.31 mb ± 17.0 %

$E_n = 8.01 \pm 0.03$ MeV
(n,n') to: 0.962 MeV Level

θ_{cm}	$d\sigma/d\omega$	Δ (%)	
deg.	*mb/str*	+	−
83.47	0.82	62.5	30.8

Avg. $d\sigma/d\omega$ = 0.82 mb/str ± 47.2 %
$\int(d\sigma/d\omega)d\omega$ = 10.25 mb ± 47.2 %

$E_n = 8.01 \pm 0.03$ MeV
(n,n') to: 1.327 MeV Level
+ 1.412 MeV Level
+ 1.547 MeV Level

θ_{cm}	$d\sigma/d\omega$	Δ (%)	
deg.	*mb/str*	+	−
83.50	2.52	29.7	27.9

Avg. $d\sigma/d\omega$ = 2.52 mb/str ± 29.7 %
$\int(d\sigma/d\omega)d\omega$ = 31.73 mb ± 29.7 %

$E_n = 8.50 \pm 0.05$ MeV
Elastic Scattering

θ_{cm}	$d\sigma/d\omega$	Δ (%)	
deg.	*mb/str*	+	−
13.10	2451.66	4.2	4.5
20.70	1839.83	5.2	5.4
27.92	954.23	4.9	6.3
28.30	993.12	7.5	6.6
35.53	435.92	5.9	6.2
43.12	131.22	9.9	8.9
48.18	33.67	13.6	15.5
55.75	4.00	67.0	59.1
63.31	12.24	27.0	20.2
70.86	23.73	16.2	12.9
78.39	30.11	11.9	13.7
83.41	29.20	8.1	8.5
85.91	23.59	18.9	12.5
90.91	23.02	15.7	11.8
93.41	19.62	10.3	13.9
98.40	15.56	11.3	13.4
100.90	13.90	15.6	15.9
108.37	8.88	18.8	18.2
119.30	6.13	24.8	23.7
126.74	3.81	37.4	41.5
134.16	4.83	36.0	30.4

$\int(d\sigma/d\omega)d\omega = 2021.02$ mb ± 7.3 %
Wick's Limit = 3262.31 mb ± 9.2 %
$\sigma_T =$ 3.60 b ± 3.0 %

Legendre Fit, Order = 9

k	a_k	Δ(%)
0	321.65503	2.2
1	273.79541	2.4
2	227.04007	2.5
3	175.76830	2.7
4	127.89275	3.0
5	78.67165	3.8
6	41.06406	5.4
7	17.54846	9.3
8	5.91547	16.5
9	1.53630	38.7

$E_n = 8.50 \pm 0.05$ MeV
(n,n') to: 1.327 MeV Level
+ 1.412 MeV Level
+ 1.547 MeV Level

θ_{cm}	$d\sigma/d\omega$	Δ (%)	
deg.	*mb/str*	+	−
85.99	2.52	34.3	34.3
119.38	1.98	32.1	32.1

Avg. $d\sigma/d\omega =$ 2.17 mb/str ± 24.8 %
$\int(d\sigma/d\omega)d\omega =$ 27.29 mb ± 24.8 %

^{65}Cu CROSS SECTIONS

$E_n = 5.50 \pm 0.09$ MeV
Elastic Scattering

θ_{cm}	$d\sigma/d\omega$	Δ (%)	
deg.	*mb/str*	+	−
13.10	2422.36	4.5	4.2
20.70	1757.25	4.8	4.7
27.91	1008.22	5.6	5.0
28.30	1121.41	5.0	5.6
35.51	535.91	5.6	6.2
43.10	221.66	6.2	7.0
48.15	115.66	7.3	9.2
55.73	31.26	12.2	20.2
63.29	22.15	23.9	20.3
70.83	44.10	10.7	14.5
78.37	58.36	9.7	15.5
83.38	63.78	8.0	12.7
85.88	60.57	13.3	12.0
90.89	56.94	12.3	10.5
93.38	48.55	18.2	8.7
98.38	49.48	10.4	10.8
100.87	44.63	8.8	12.0
108.35	32.52	13.8	13.4
119.28	20.30	13.6	16.7
126.72	11.50	21.8	19.4
134.14	8.09	27.9	26.3

$\int(d\sigma/d\omega)d\omega = 2294.11$ mb ± 7.2 %
Wick's Limit = 2354.23 mb ± 9.2 %
$\sigma_T = 3.80$ b ± 3.0 %

Legendre Fit, Order = 8

k	a_k	Δ(%)
0	365.11890	1.9
1	283.26440	2.2
2	214.48798	2.5
3	164.53285	2.6
4	112.23418	3.0
5	58.81996	4.5
6	24.64420	8.2
7	7.48998	18.7
8	1.65033	52.4

$E_n = 5.50 \pm 0.09$ MeV
(n,n′) to: 1.115 MeV Level

θ_{cm}	$d\sigma/d\omega$	Δ (%)	
deg.	*mb/str*	+	−
43.17	6.03	33.4	41.3
48.24	4.71	31.9	39.5
55.82	4.07	29.5	43.9
70.93	2.73	47.5	41.2
78.47	4.14	23.9	37.9
83.49	3.97	35.6	42.2
90.99	4.34	28.3	40.7
93.50	3.24	55.6	34.0
98.49	3.39	37.0	39.9
100.98	3.67	28.4	37.9

Avg. $d\sigma/d\omega = 3.78$ mb/str ± 15.1 %
$\int(d\sigma/d\omega)d\omega = 47.44$ mb ± 15.1 %

$E_n = 5.50 \pm 0.09$ MeV
(n,n′) to: 1.481 MeV Level
+ 1.620 MeV Level
+ 1.720 MeV Level

θ_{cm}	$d\sigma/d\omega$	Δ (%)	
deg.	*mb/str*	+	−
35.60	11.02	35.6	30.7
43.21	7.72	17.9	31.2
48.28	7.38	19.0	37.9
55.86	6.62	23.2	30.8
63.43	7.15	10.1	30.9
70.99	7.31	10.4	34.9
78.53	6.70	18.5	29.7
83.53	6.46	16.5	29.1
91.05	8.16	10.6	27.2
93.55	6.15	17.3	26.2
98.54	7.44	10.7	24.9
101.03	6.45	16.3	27.9
119.43	4.61	46.1	25.8
126.85	5.60	11.0	30.3

Avg. $d\sigma/d\omega = 6.22$ mb/str ± 10.3 %
$\int(d\sigma/d\omega)d\omega = 78.20$ mb ± 10.3 %

$E_n = 6.00 \pm 0.04$ MeV
(n,n′) to: 1.115 MeV Level

θ_{cm}	$d\sigma/d\omega$	Δ (%)	
deg.	*mb/str*	+	−
83.48	4.34	21.0	35.1
90.98	3.48	20.2	33.1
98.48	4.62	10.7	29.1

Avg. $d\sigma/d\omega$ = 3.80 mb/str ± 17.0 %
$\int(d\sigma/d\omega)d\omega$ = 47.80 mb ± 17.0 %

$E_n = 6.00 \pm 0.04$ MeV
(n,n′) to: 1.481 MeV Level
+ 1.620 MeV Level
+ 1.720 MeV Level

θ_{cm}	$d\sigma/d\omega$	Δ (%)	
deg.	*mb/str*	+	−
83.52	5.75	9.8	24.1
91.03	5.93	19.1	29.6
98.52	5.94	15.0	31.0

Avg. $d\sigma/d\omega$ = 5.78 mb/str ± 11.5 %
$\int(d\sigma/d\omega)d\omega$ = 72.63 mb ± 11.5 %

$E_n = 6.49 \pm 0.04$ MeV
(n,n′) to: 1.115 MeV Level

θ_{cm}	$d\sigma/d\omega$	Δ (%)	
deg.	*mb/str*	+	−
83.47	3.26	21.6	32.2
90.97	3.26	14.6	27.4
98.47	3.38	19.5	34.1

Avg. $d\sigma/d\omega$ = 3.27 mb/str ± 13.7 %
$\int(d\sigma/d\omega)d\omega$ = 41.13 mb ± 13.7 %

$E_n = 6.49 \pm 0.04$ MeV
(n,n′) to: 1.481 MeV Level
+ 1.620 MeV Level
+ 1.720 MeV Level

θ_{cm}	$d\sigma/d\omega$	Δ (%)	
deg.	*mb/str*	+	−
83.50	5.18	19.3	26.8
91.01	5.21	15.0	26.8
98.51	4.43	12.3	33.0

Avg. $d\sigma/d\omega$ = 4.60 mb/str ± 12.8 %
$\int(d\sigma/d\omega)d\omega$ = 57.74 mb ± 12.8 %

$E_n = 7.00 \pm 0.06$ MeV
Elastic Scattering

θ_{cm}	$d\sigma/d\omega$	Δ (%)	
deg.	*mb/str*	+	−
13.10	2832.61	3.8	5.1
20.70	2093.54	3.8	7.4
27.91	1111.71	4.7	5.7
28.30	1218.05	4.6	6.4
35.51	514.77	5.9	6.2
43.10	185.82	11.3	8.7
48.16	83.90	8.9	9.9
55.73	15.93	19.1	26.4
63.29	18.50	17.4	22.9
70.83	42.67	10.0	10.2
78.36	50.60	10.3	9.8
83.38	53.23	7.6	10.4
85.88	46.86	8.0	11.4
90.89	43.16	8.1	9.4
93.39	33.63	8.6	13.7
98.38	29.50	10.7	10.9
100.87	23.90	9.8	15.1
108.35	13.50	14.3	21.8
119.28	7.42	22.0	23.8
126.72	7.03	23.4	24.8
134.14	3.85	43.2	46.1

$\int(d\sigma/d\omega)d\omega = 2380.66$ mb $\pm$ 7.3 %
Wick's Limit $= 2917.97$ mb $\pm$ 9.2 %
$\sigma_T = 3.75$ b $\pm$ 3.0 %

Legendre Fit, Order = 8

k	a_k	Δ(%)
0	378.89355	2.1
1	314.23389	2.3
2	246.53348	2.5
3	188.26891	2.7
4	132.39656	2.9
5	76.09474	3.8
6	34.31850	6.0
7	11.19480	11.3
8	2.85958	24.5

$E_n = 7.00 \pm 0.06$ MeV
(n,n') to: 1.115 MeV Level

θ_{cm}	$d\sigma/d\omega$	Δ (%)	
deg.	*mb/str*	+	−
48.21	2.85	44.9	39.4
55.79	2.29	64.7	33.0
78.44	2.09	55.7	37.9

Avg. $d\sigma/d\omega = 2.44$ mb/str $\pm$ 30.1 %
$\int(d\sigma/d\omega)d\omega = 30.69$ mb $\pm$ 30.1 %

$E_n = 7.00 \pm 0.06$ MeV
(n,n') to: 1.481 MeV Level
+ 1.620 MeV Level
+ 1.720 MeV Level

θ_{cm}	$d\sigma/d\omega$	Δ (%)	
deg.	*mb/str*	+	−
48.25	6.12	11.5	32.8
55.82	3.54	42.8	22.3
63.39	3.24	28.3	30.0
70.95	2.73	33.2	27.6
78.48	3.55	20.6	31.3
83.49	4.52	17.4	28.8
91.00	4.17	20.9	28.7
100.99	3.94	16.5	30.0
108.46	2.70	36.0	30.8

Avg. $d\sigma/d\omega = 3.51$ mb/str $\pm$ 12.8 %
$\int(d\sigma/d\omega)d\omega = 44.05$ mb $\pm$ 12.8 %

$E_n = 7.50 \pm 0.03$ MeV
(n,n') to: 1.481 MeV Level
+ 1.620 MeV Level
+ 1.720 MeV Level

θ_{cm}	$d\sigma/d\omega$	Δ (%)	
deg.	*mb/str*	+	−
83.49	3.98	16.4	34.5
91.00	3.19	17.4	32.9
98.48	3.78	12.0	28.8

Avg. $d\sigma/d\omega = 3.38$ mb/str $\pm$ 15.7 %
$\int(d\sigma/d\omega)d\omega = 42.49$ mb $\pm$ 15.7 %

$E_n = 8.50 \pm 0.05$ MeV
Elastic Scattering

θ_{cm}	$d\sigma/d\omega$	Δ (%)	
deg.	*mb/str*	+	−
13.10	2638.89	5.3	4.6
20.70	1968.84	5.7	4.7
27.91	936.89	4.5	5.6
28.30	997.44	5.2	6.3
35.51	426.81	5.1	5.9
43.10	125.05	6.6	8.6
48.15	37.61	14.6	14.9
55.73	8.36	28.4	37.1
63.29	15.64	17.0	19.1
70.83	32.90	15.3	11.7
78.37	36.68	11.6	17.9
85.88	33.77	9.1	14.9
93.39	24.88	8.5	17.3
100.87	15.73	15.1	16.3
108.35	8.82	16.6	20.9
119.28	7.76	20.9	17.9
126.72	6.84	21.5	26.9
134.14	7.15	24.4	24.6

$\int(d\sigma/d\omega)d\omega = 2114.36$ mb $\pm$ 7.3 %
Wick's Limit = 3265.46 mb $\pm$ 9.2 %
$\sigma_T =$ 3.60 b $\pm$ 3.0 %

Legendre Fit, Order = 9

k	a_k	Δ(%)
0	336.51172	2.2
1	282.43335	2.4
2	233.98256	2.6
3	182.15776	2.8
4	134.69217	3.1
5	84.46579	3.8
6	44.95248	5.3
7	20.08553	8.9
8	7.84700	13.9
9	2.47074	27.7

$E_n = 8.50 \pm 0.05$ MeV
(n,n') to: 1.481 MeV Level
+ 1.620 MeV Level
+ 1.720 MeV Level

θ_{cm}	$d\sigma/d\omega$	Δ (%)	
deg.	*mb/str*	+	−
48.22	2.40	52.3	22.1
55.80	2.78	27.7	29.5
63.37	2.75	23.7	34.9
100.96	2.24	31.8	28.1
126.79	1.71	22.8	30.0

Avg. $d\sigma/d\omega =$ 2.13 mb/str $\pm$ 14.4 %
$\int(d\sigma/d\omega)d\omega =$ 26.82 mb $\pm$ 14.4 %

ORNL-4908
UC-79d
(ENDF-203)

INTERNAL DISTRIBUTION

1–3. Central Research Library
4. ORNL – Y-12 Technical Library Document Reference Section
5–24. Laboratory Records Department
25. Laboratory Records, ORNL R.C.
26–28. L. S. Abbott
29. R. G. Alsmiller, Jr.
30. C. E. Clifford
31. F. L. Culler
32. J. K. Dickens
33. C. Y. Fu
34. W. O. Harms
35. R. F. Hibbs
36–45. W. E. Kinney
46. T. A. Love
47–48. F. C. Maienschein
49. G. L. Morgan
50. F. R. Mynatt
51. E. M. Oblow
52. R. W. Peelle
53. S. K. Penny
54–68. F. G. Perey
69. Herman Postma
70. R. W. Roussin
71. M. J. Skinner
72. A. M. Weinberg
73. A. Zucker
74. H. Feshbach (Consultant)
75. P. F. Fox (Consultant)
76. W. W. Haven, Jr. (Consultant)
77. A. F. Henry (Consultant)

EXTERNAL DISTRIBUTION

78–79. USAEC Division of Reactor Research and Development, Washington, D.C. 20545
80. USAEC-RRD Senior Site Representative, ORNL
81. Research and Technical Support Division, AEC, ORO
82. Patent Office, AEC, ORO
83–309. Given distribution as shown in TID-4500 under UC-79d, Liquid Metal Fast Breeder Reactors (Physics)
310–369. Technical Information Center for ENDF distribution